Density-functional expansion methods: Generalization of the auxiliary basis

Timothy J. Giese and Darrin M. York[a)]
BioMaPS Institute and Department of Chemistry and Chemical Biology, Rutgers University, Piscataway, New Jersey 08854-8087, USA

(Received 14 February 2011; accepted 14 April 2011; published online 16 May 2011)

The formulation of density-functional expansion methods is extended to treat the second and higher-order terms involving the response density and spin densities with an arbitrary single-center auxiliary basis. The two-center atomic orbital products are represented by the auxiliary functions centered about those two atoms, and the mapping coefficients are determined from a local constrained variational procedure. This two-center variational procedure allows the mapping coefficients to be pretabulated and splined as a function of internuclear separation for efficient look up. The splines of mapping coefficients have a range no longer than that of the overlap integrals, and the auxiliary density appears as a single point-multipole expansion to all nonoverlapping atoms, thus allowing for the trivial implementation of a linear-scaling algorithm. The method is tested using Gaussian multipole expansions, and the effect of angular and radial completeness is explored. Several auxiliary basis sets are parametrized and compared to an auxiliary basis analogous to that used in the self-consistent-charge density-functional tight-binding model, and the method is demonstrated to greatly improve the representation of the density response with respect to a reference expansion model that does not use an auxiliary basis. © *2011 American Institute of Physics*. [doi:10.1063/1.3587052]

I. INTRODUCTION

Density-functional expansion methods are derivable from an integral Taylor series expansion of the Kohn-Sham potential energy, and the currently most popular variant is the self-consistent-charge density-functional tight-binding (SCC-DFTB) model.[1–4] Although SCC-DFTB has proven to be a very useful semiempirical model,[5–8] there remain open questions as to which theoretical developments will result in the most beneficial improvements.[3] For example, one of the recent improvements[4,9] introduced charge-dependent corrections through the inclusion of higher-order expansion terms, i.e., beyond second-order; however, in a recent work,[10] we explored the theory and approximations used in *de novo* density-functional expansion methods and concluded that a second-order potential energy expansion reproduces standard density functional theory (DFT) results extremely well if the model is not encumbered by the following approximations: (1) the two-body treatment of the first-order matrix elements, (2) the Slater monopole auxiliary basis representation of the response density, and (3) the limited size of the orbital basis. These approximations are used in SCC-DFTB for computational efficiency, but also pose severe limitations to the accuracy that can be achieved. The empirical corrections presented in Refs. 4 and 11 promise to be quite useful in masking the detrimental effects of these approximations; however, one should take care not to misconstrue the ability of a third-order model to reduce errors by attributing the primary reason for the presence of those errors to a premature truncation of the Taylor series expansion. Such attribution can only be made in the absence of the other, much more severe, approximations. Thus we feel that further investigation into the above three approximations is warranted and will lead to further insight and advancement of the models.

Recent work in the development of SCC-DFTB has focused on the pragmatic advancement of the model, and has resulted in new, efficient, and ever-improving methods,[4,12–14] parameters,[9,15–18] and computer codes.[2,19,20] The approach we have chosen is quite different, in that we start from an *ab initio*-like model that reproduces DFT results very well without the use of parameters, and then identify where and quantify by how much the model breaks down when various approximations are introduced. This information is then used to motivate the design of new, computationally efficient, and physically realistic quantum models that retains high accuracy with only a minimal reliance on empirical parameters. One must recognize that a next-generation approximate DFT method that overcomes the three limitations listed above will ultimately require some parametrization, and will certainly be more computationally expensive than current SCC-DFTB methods. In this sense, our development is complimentary to the ongoing improvements of SCC-DFTB.

This paper focuses on the description of the response density through the use of an auxiliary basis. SCC-DFTB uses a Slater monopole auxiliary basis whose charges are determined from Mulliken partitioning. By using this type of auxiliary basis, SCC-DFTB avoids the need for computing three- and four-center electron repulsion integrals, and Mulliken partitioning allows for the rapid construction of the auxiliary density from the atomic orbital (AO) density matrix through spline evaluation of the precomputed overlap matrices; however, this crude representation of the response density can have adverse effects on electrostatic interactions.[21] In general, accurate electrostatics are important for intermolecular

a)Electronic mail: york@biomaps.rutgers.edu.

interactions, and in particular, hydrogen bonding.[22,23] Variations of the SCC-DFTB method have been applied to water clusters,[24] liquid water,[24] and organic molecules,[6] and limitations in hydrogen bonding were noted in many cases, although it is difficult to directly attribute these deficiencies solely to the electrostatic description.

To extend the auxiliary basis to higher-order multipoles, one must develop a formalism that can rapidly compute the coefficients used to represent the AO products with the auxiliary functions. Fortunately, there has been much interest in the use of auxiliary basis sets in the context of traditional *ab initio* methods[25–30] and polarizable density-fitted force fields,[31–34] whose ideas we can draw upon. In the context of Kohn-Sham potential energy expansion methods, however, we seek to tailor the methodology to allow for the precomputation of these "mapping coefficients" on numerical splines, in a manner analogous to SCC-DFTB.

The formulation presented here is valid for an arbitrary single-center auxiliary and AO basis, and requires at most two-center integrals. This differs from most "resolution of the identity" methods, which require three-center integrals.[25,26,29,35–38] In brief, each AO product is represented as a sum of auxiliary functions on either one (for coincident center AO products) or two atoms (for two-center AO products). The coefficients which map the AO products onto single-center auxiliary functions can be splined as a function of atom separation and their interpolated values are rotated into the desired orientation. The rotated mapping coefficients can be computed once before the self-consistent field (SCF) procedure starts, and thus the most computationally demanding aspects of this generalization are not compounded by the number of SCF iterations required to reach convergence. The numerical splines of mapping coefficients have a range no greater than those of the overlap matrix. Thus, their evaluation need only be performed over a petite list of near-neighbors. Furthermore, the auxiliary density will appear as a single point multipole expansion to all nonoverlapping atoms. The importance of these two combined characteristics should not be overlooked, as this allows for a trivial implementation of a linear-scaling algorithm.[35,39–41]

Our description of the auxiliary basis representation of the AO products is a very useful starting point for the description of other models and extensions of SCC-DFTB. We describe the nonlinear potential energy corrections as a general functional of the response density and spin densities and transform it into a function of atom positions, auxiliary moments of response charge density, and auxiliary moments of spin charge density. With this transformation, the Fock matrix elements are derived and it is shown that the expression depends only on the mapping coefficients and the vectors of auxiliary potentials and spin potentials, which are the derivatives of the energy with respect to the vectors of auxiliary moments and auxiliary spin moments, respectively. Thus, when describing a new energy functional that depends on the auxiliary representation of the density and spin densities, it is not necessary to derive expressions for the Fock matrix elements; one need only derive expressions for the auxiliary potentials.

Furthermore, we describe the mechanism that we have used for generating the mapping coefficient splines; we explore the effect of angular momentum and radial completeness of the auxiliary basis on response properties; and we parametrize an auxiliary basis using a limited number of auxiliary functions, and explore its ability to reproduce molecular geometries, dipole moments, bond energies, and the potential energy surface of a water dimer.

II. METHODS

A. Auxiliary basis representation of atomic orbital products

The energy of a Kohn-Sham expansion model[10,42,43] evaluated about a spin-paired reference density can be written as

$$E = \sum_{ij} P_{ij} T_{ij} + V^{(0)}(\mathbf{R}) + \sum_{ij} \left(P_{ij} - P_{ij}^{(0)}\right) V_{ij}^{(1)} + W[\delta\rho, \omega], \tag{1}$$

where $\mathbf{P}$ and $\mathbf{P}^{(0)}$ are the single particle density and reference density matrices in the AO basis $\{\chi\}$, respectively; $\mathbf{T}$ is the kinetic energy matrix; $V^{(0)}(\mathbf{R})$ is the reference potential energy, which depends on a reference density, assumed here to be a sum of reference atomic densities that are centered about and follow their respective atomic positions, denoted collectively by $\mathbf{R}$;

$$V_{ij}^{(1)} = \int \left[\frac{\delta V[\rho, \omega]}{\delta\rho(\mathbf{r})}\right]_0 \chi_i(\mathbf{r})\chi_j(\mathbf{r}) d^3r, \tag{2}$$

is the first-order density response potential energy matrix;[44] $V[\rho, \omega]$ is the Kohn-Sham potential energy functional;[45] the subscript "0" outside the functional derivative indicates that it is evaluated about the spin-averaged reference $[\rho(\mathbf{r}) = \rho_{\text{ref}}(\mathbf{r})$ and $\omega(\mathbf{r}) = 0]$; and $W[\delta\rho, \omega]$ is a quantity that describes all second and higher-order terms of the response density.[4] These functionals take as arguments the total density response $\delta\rho(\mathbf{r})$ and spin density $\omega(\mathbf{r})$, which are related to the spin-resolved density matrices and AO basis

$$\delta\rho(\mathbf{r}) = \sum_{ij} \left(P_{ij}^{\alpha} + P_{ij}^{\beta} - P_{ij}^{(0)}\right) \chi_i(\mathbf{r})\chi_j(\mathbf{r}), \tag{3}$$

$$\omega(\mathbf{r}) = \sum_{ij} \left(P_{ij}^{\alpha} - P_{ij}^{\beta}\right) \chi_i(\mathbf{r})\chi_j(\mathbf{r}), \tag{4}$$

which in turn are related to the molecular orbital coefficients $\mathbf{C}^{\sigma}$ and orbital occupation numbers $\mathbf{n}^{\sigma}$

$$P_{ij}^{\sigma} = \sum_{k} n_k^{\sigma} C_{ik}^{\sigma} C_{jk}^{\sigma}, \tag{5}$$

arising from the solution of the generalized eigenvalue problem[46]

$$\mathbf{F}^{\sigma} \cdot \mathbf{C}^{\sigma} = \mathbf{S} \cdot \mathbf{C}^{\sigma} \cdot \mathbf{E}^{\sigma}, \tag{6}$$

where

$$F_{ij}^{\sigma} = \frac{dE}{dP_{ij}^{\sigma}} \tag{7}$$

is the spin-resolved Fock matrix and $\mathbf{S}$ is the overlap matrix.

From the above equations, the energy can be minimized by performing a standard SCF procedure. The expression for the Fock matrix upon inserting Eq. (1) into (7) is

$$F_{ij}^{\sigma} = T_{ij} + V_{ij}^{(1)} + \int \frac{\delta W[\delta\rho, \omega]}{\delta\rho(\mathbf{r})} \chi_i(\mathbf{r})\chi_j(\mathbf{r}) d^3r + (-1)^{\delta_{\sigma,\beta}} \int \frac{\delta W[\delta\rho, \omega]}{\delta\omega(\mathbf{r})} \chi_i(\mathbf{r})\chi_j(\mathbf{r}) d^3r, \quad (8)$$

however, the last two integrals are inconvenient to analytically evaluate within semiempirical models because, as it is known that $W[\delta\rho, \omega]$ contains a Coulomb component, one would formally need to compute three- and four-center electron repulsion integrals.[47] Of course, certain approximations or numerical techniques[41,48,49] can reduce the evaluation of the Coulomb component to $O(N \log N)$, and we describe now a general technique to simplify these integrals within Kohn-Sham expansion methods.

To avoid the need for computing three- or four-center integrals, one can approximate each product of AOs by a sum of single-center auxiliary functions $\{\varphi\}$

$$\chi_i(\mathbf{r} - \mathbf{R}_a)\chi_j(\mathbf{r} - \mathbf{R}_b) = \begin{cases} \sum_{k\in a} M_{ijk}^a \varphi_k(\mathbf{r} - \mathbf{R}_a), & \text{if } a = b \\ \sum_{k\in a} M_{ijk}^a \varphi_k(\mathbf{r} - \mathbf{R}_a) + \sum_{k\in b} M_{ijk}^b \varphi_k(\mathbf{r} - \mathbf{R}_b), & \text{otherwise,} \end{cases} \quad (9)$$

where the $\mathbf{M}^a$'s and $\mathbf{M}^b$'s are coefficients that map the AO basis product onto the auxiliary basis of atoms a and b, respectively. In principle, all auxiliary basis functions in the system could be used to represent each AO basis product; however, this would require evaluation of three-center integrals.[26,50] By limiting the auxiliary representation to those atoms involved in the AO product, the mapping coefficients can be splined as a function of atom separation.

We defer the description of our method for determining the mapping coefficients for the time being, but as an explanatory example, we relate the above equation to SCC-DFTB. SCC-DFTB uses a single monopole auxiliary basis and this choice of basis provides a simple mechanism for obtaining the mapping coefficients. A Mulliken charge partitioning[51] is equivalent to writing

$$M_{ij1}^a = S_{ij}, \quad \text{for } i \in a,\ j \in a, \quad (10)$$

and

$$M_{ij1}^a = M_{ij1}^b = \frac{1}{2} S_{ij}, \quad \text{for } i \in a,\ j \in b, \quad (11)$$

although alternative mapping procedures, such as those used by the CM3 "class IV" charge model, are possible and have been used with SCC-DFTB as well.[52]

The single-center auxiliary basis allows us to write the response density as a sum of auxiliary functions and associated auxiliary moments of response charge density $\mathbf{m}$ and spin charge density $\mathbf{s}$

$$\delta\rho(\mathbf{r}) = -\sum_a \sum_k m_k^a \varphi_k(\mathbf{r} - \mathbf{R}_a) \quad (12)$$

$$\omega(\mathbf{r}) = -\sum_a \sum_k s_k^a \varphi_k(\mathbf{r} - \mathbf{R}_a), \quad (13)$$

where the auxiliary charge and spin charge moments of auxiliary function k on atom a are

$$m_k^a = -\sum_{i\in a}\sum_{j\in a} \left(P_{ij} - P_{ij}^{(0)}\right) M_{ijk}^a - \sum_{i\in a}\sum_{j\notin a} \left(P_{ij} - P_{ij}^{(0)}\right) M_{ijk}^a - \sum_{i\notin a}\sum_{j\in a} \left(P_{ij} - P_{ij}^{(0)}\right) M_{ijk}^a \quad (14)$$

and

$$s_k^a = -\sum_{i\in a}\sum_{j\in a} \left(P_{ij}^{\alpha} - P_{ij}^{\beta}\right) M_{ijk}^a - \sum_{i\in a}\sum_{j\notin a} \left(P_{ij}^{\alpha} - P_{ij}^{\beta}\right) M_{ijk}^a - \sum_{i\notin a}\sum_{j\in a} \left(P_{ij}^{\alpha} - P_{ij}^{\beta}\right) M_{ijk}^a. \quad (15)$$

The leading minus signs in Eqs. (12)–(15) appear as a part of the transformation between electron density and charge density representations.

One can rewrite the last term in Eq. (1) so that it is a function of each atom's $\mathbf{m}$'s, $\mathbf{s}$'s, and atom position, as opposed to a functional of $\delta\rho(\mathbf{r})$ and $\omega(\mathbf{r})$, i.e., $W[\delta\rho, \omega] \rightarrow W(\mathbf{m}^a, \mathbf{m}^b, \ldots, \mathbf{m}^n, \mathbf{s}^a, \mathbf{s}^b, \ldots, \mathbf{s}^n, \mathbf{R})$; however, for ease of notation we will indicate that the function depends on the auxiliary moments of all atoms by dropping the atom index superscript, e.g., $W(\mathbf{m}, \mathbf{s}, \mathbf{R})$. As an example of this transformation, the Coulomb functional

$$J[\delta\rho] = \frac{1}{2} \int\int \frac{\delta\rho(\mathbf{r})\delta\rho(\mathbf{r}')}{|\mathbf{r} - \mathbf{r}'|} d^3r d^3r' \quad (16)$$

becomes

$$J(\mathbf{m}, \mathbf{R}) = \sum_a \sum_b \sum_{k\in a} \sum_{k'\in b} m_k^a m_{k'}^b \times \frac{1}{2} \int\int |\mathbf{r} - \mathbf{r}'|^{-1} \times \varphi_k(\mathbf{r} - \mathbf{R}_a)\varphi_{k'}(\mathbf{r}' - \mathbf{R}_b) d^3r d^3r'. \quad (17)$$

Upon applying this transformation to $W[\delta\rho, \omega]$, the Fock matrix [Eq. (7)] is

$$F_{ij}^{\sigma} = T_{ij} + V_{ij}^{(1)} + \sum_a \sum_k \frac{\partial W(\mathbf{m}, \mathbf{s}, \mathbf{R})}{\partial m_k^a} \frac{dm_k^a}{dP_{ij}^{\sigma}} + \sum_a \sum_k \frac{\partial W(\mathbf{m}, \mathbf{s}, \mathbf{R})}{\partial s_k^a} \frac{ds_k^a}{dP_{ij}^{\sigma}}, \tag{18}$$

where the required derivatives [from Eqs. (14)–(15)] are

$$\frac{dm_k^a}{dP_{ij}^{\sigma}} = \begin{cases} -M_{ijk}^a, & \text{if } i \in a \text{ or } j \in a \\ 0, & \text{otherwise,} \end{cases} \tag{19}$$

$$\frac{ds_k^a}{dP_{ij}^{\sigma}} = \begin{cases} -(-1)^{\delta_{\sigma,\beta}} M_{ijk}^a, & \text{if } i \in a \text{ or } j \in a \\ 0, & \text{otherwise,} \end{cases} \tag{20}$$

and if we define the auxiliary charge potential

$$p_k^a = \frac{\partial W(\mathbf{m}, \mathbf{s}, \mathbf{R})}{\partial m_k^a}, \tag{21}$$

and auxiliary spin charge potential

$$w_k^a = \frac{\partial W(\mathbf{m}, \mathbf{s}, \mathbf{R})}{\partial s_k^a}, \tag{22}$$

we arrive at

$$F_{ij}^{\sigma} = \begin{cases} T_{ij} + V_{ij}^{(1)} - \sum_{k \in a} \phi_k^{a,\sigma} M_{ijk}^a, & \text{if } i, j \in a \\ T_{ij} + V_{ij}^{(1)} - \sum_{k \in a} \phi_k^{a,\sigma} M_{ijk}^a - \sum_{k \in b} \phi_k^{b,\sigma} M_{ijk}^b, & \text{if } i \in a \text{ and } j \in b, \end{cases} \tag{23}$$

where

$$\phi_k^{a,\sigma} = p_k^a + (-1)^{\delta_{\sigma,\beta}} w_k^a \tag{24}$$

is a spin-resolved auxiliary charge potential.

To summarize, the procedure for computing the Fock matrix is:

- Compute the $\mathbf{T}$, $\mathbf{V}^{(1)}$, and the density matrices [Eq. (5)].
- Form the auxiliary moments from the mapping coefficients and density matrices [Eqs. (14) and (15)].
- Compute the auxiliary potentials [Eqs. (21) and (22)].
- Compute the spin-resolved auxiliary potentials [Eq. (24)]
- Map the spin-resolved auxiliary potentials into the Fock matrices [Eq. (23)].

The above formalism makes it very convenient to create new functional forms of $W(\mathbf{m}, \mathbf{s}, \mathbf{R})$ because the mechanism for incorporating its contribution to the Fock matrix is well defined, and one need only derive expressions for the auxiliary potentials [Eqs. (21) and (22)].

B. Calculation of the mapping coefficients

Our approach for computing the mapping coefficients is to pretabulate them for one-center AO products and to generate numerical splines for the two-center AO products. When the angular dependence of both the AO and auxiliary basis are described by spherical harmonics and the atom pairs are aligned along the z-axis, many of the mapping coefficients vanish due to symmetry. Thus, only the nonzero mapping coefficients must be stored on numerical splines. To obtain the two-center mapping coefficient matrix from the pretabulated splines, one first zeros the mapping coefficient matrix, fills in the non-zero elements by spline look up, and then performs a series of spherical harmonic rotations into the desired orientation. To perform the rotation, a single, block-diagonal unitary matrix of real-valued Wigner-D matrices can be efficiently computed from recurrence relations.[53] The calculation of this matrix requires the 3×3 matrix that rotates a vector pointing along the z-axis to a vector pointing along the desired internuclear vector $\mathbf{R}_{ab}$. This rotation matrix is defined by $\mathbf{R}_{ab}$, and hence we notate a diagonal block of the unitary matrix by $\mathbf{D}^l(\mathbf{R}_{ab})$, where l is the angular momentum order of the block. Each AO and auxiliary radial function, when multiplied by spherical harmonics, forms a shell of $2l + 1$ functions of common angular momentum l, and the three-index matrix $\mathbf{M}^a$ can be partitioned into three-index blocks of shells, where a block has dimensions $(2l_i + 1)(2l_j + 1)(2l_k + 1)$. In this context, i, j, and k represent indices of orbital blocks i and j and auxiliary block k. The elements μ_i, μ_j, and μ_k within the ijk-block in the $\mathbf{R}_{ab}$-oriented frame $[M^a_{\mu_i,\mu_j,\mu_k}(\mathbf{R}_{ab})]$ are related to the ijk-block in the $\mathbf{Z}_{ab}$-oriented frame $[M^a_{\mu_i,\mu_j,\mu_k}(\mathbf{Z}_{ab})]$ by

$$M^a_{\mu_i,\mu_j,\mu_k}(\mathbf{R}_{ab}) = \sum_{\mu_i'} \sum_{\mu_j'} \sum_{\mu_k'} D^{l_i}_{\mu_i,\mu_i'}(\mathbf{R}_{ab}) \times D^{l_j}_{\mu_j,\mu_j'}(\mathbf{R}_{ab}) D^{l_k}_{\mu_k,\mu_k'}(\mathbf{R}_{ab}) \times M^a_{\mu_i',\mu_j',\mu_k'}(\mathbf{Z}_{ab}). \tag{25}$$

The elements of $\mathbf{M}^b$ rotate in the same way; the expression differs from above by replacing $M^a_{\mu_i,\mu_j,\mu_k}(\mathbf{R}_{ab})$ and $M^a_{\mu_i',\mu_j',\mu_k'}(\mathbf{Z}_{ab})$ with $M^b_{\mu_i,\mu_j,\mu_k}(\mathbf{R}_{ab})$ and $M^b_{\mu_i',\mu_j',\mu_k'}(\mathbf{Z}_{ab})$, respectively.

The mapping coefficients of orbital product i and j on atoms a and b separated by $\mathbf{Z}_{ab}$ along the z-axis are computed from a constrained electrostatic fitting procedure. For this AO product and atom separation, we seek to determine all k in M^a_{ijk} and M^b_{ijk}, which we represent collectively by the vector $\mathbf{M}$. Suppose that atoms a and b had $N_{\text{aux},a}$ and $N_{\text{aux},b}$ auxiliary functions, respectively, then the first $N_{\text{aux},a}$ elements of $\mathbf{M}$ would correspond to all k in M^a_{ijk} and the last $N_{\text{aux},b}$

elements being those k in M^b_{ijk}. The auxiliary representation of the ij AO product is exact when the electrostatic potential of the auxiliary representation matches the electrostatic potential of the AO product everywhere. This implies the variational condition[26,54]

$$\delta \left\{ \mathbf{M}^T \cdot \mathbf{g} - \frac{1}{2}\mathbf{M}^T \cdot \eta \cdot \mathbf{M} - (\mathbf{M}^T \cdot \mathbf{D} - \mathbf{d}^T) \cdot \mathbf{u} \right\} = 0, \tag{26}$$

where

$$g_k = \int\int \frac{\varphi_k(\mathbf{r}-\mathbf{R}_k)}{|\mathbf{r}-\mathbf{r}'|} \times \chi_i(\mathbf{r}'-\mathbf{R}_a)\chi_j(\mathbf{r}'-\mathbf{R}_b)d^3r d^3r', \tag{27}$$

$$\eta_{k,k'} = \int\int \frac{\varphi_k(\mathbf{r}-\mathbf{R}_k)\varphi_{k'}(\mathbf{r}-\mathbf{R}_{k'})}{|\mathbf{r}-\mathbf{r}'|} d^3r d^3r', \tag{28}$$

and $\mathbf{R}_k$ and $\mathbf{R}_{k'}$ are either $\mathbf{R}_a$ or $\mathbf{R}_b$, depending on whether that element k is associated with the expansion on atom a or b, respectively.

The vector $\mathbf{u}$ is a set of Lagrange multipliers enforcing multipole moment constraints, i.e., an element of $\mathbf{d}$ is the multipole moment of the AO product

$$d_{(l,\mu)} = \int \chi_i(\mathbf{r}-\mathbf{R}_a)\chi_j(\mathbf{r}-\mathbf{R}_b)C_{l,\mu}(\mathbf{r})d^3r, \tag{29}$$

where $C_{l,\mu}(\mathbf{r})$ is a real regular solid harmonic and

$$D_{(l,\mu),k} = \int \varphi_k(\mathbf{r}-\mathbf{R}_k)C_{l,\mu}(\mathbf{r})d^3r \tag{30}$$

is the corresponding multipole moment of the auxiliary function.

The solution to the electrostatic fit is

$$\mathbf{M} = \eta^{-1} \cdot (\mathbf{g} - \mathbf{D} \cdot \mathbf{u}) \tag{31}$$

where

$$\mathbf{u} = \left(\mathbf{D}^T \cdot \eta^{-1} \cdot \mathbf{D}\right)^{-1} \cdot \left(\mathbf{D}^T \cdot \eta^{-1} \cdot \mathbf{g} - \mathbf{d}\right). \tag{32}$$

The number of multipole moments that we constrain depends on the choice of auxiliary functions, and the constraints are chosen in a manner that avoids having to solve an overdetermined linear equation. Each atom has a set of auxiliary functions, each with some angular momentum; let $l_{\max,a}$ and $l_{\max,b}$ be the maximum angular momentum within the set of auxiliary functions on atoms a and b, respectively. Furthermore, let $l_{\max,ab} = \max(l_{\max,a}, l_{\max,b})$ and $l_{\min,ab} = \min(l_{\max,a}, l_{\max,b})$. We include all angular components (l, μ) in Eqs. (29) and (30) from $l = 0$ to $l = l_{\max,ab}$ and those components μ in $l = l_{\max,ab} + 1$ for which $|\mu| \leq l_{\min,ab}$. Thus, there are a total of $(l_{\max,ab} + 1)^2 + 2l_{\min,ab} + 1$ constraints. As an example, suppose that both atoms used monopole auxiliary functions only. In this case, we constrain the mapping coefficients to preserve the value of the AO product overlap integral and the dipole moment along the internuclear axis. In the event that each atom contained a *single* monopole auxiliary function only, the constraints uniquely define the solution.

The tabulation of the one-center mapping coefficients is similar to above; however, there is only one set of auxiliary functions (those coincident with the orbital product), and there are only $(l_{\max,a} + 1)^2$ constraints.

C. Functional form of the auxiliary basis

Our choice of auxiliary basis $\{\varphi\}$ is a set of real-valued contracted Gaussian multipole expansions[55] (GME) of the form

$$\varphi_{l,\mu}(\mathbf{r}-\mathbf{R}_a;\xi) = \frac{C_{l,\mu}(\nabla_a)}{(2l-1)!!}\sum_{\gamma=1}^{3} c_\gamma \times \left(\frac{\zeta_\gamma(\xi)}{\pi}\right)^{3/2} e^{-\zeta_\gamma(\xi)|\mathbf{r}-\mathbf{R}_a|^2}, \tag{33}$$

where $C_{l,\mu}(\nabla_a)$ is a spherical tensor gradient operator[56,57] (STGO) acting on $\mathbf{R}_a$, and the three contraction coefficients $c_1 = 0.362052775509$, $c_2 = 0.626205052863$, $c_3 = 0.011742171628$ and primitive exponents (a.u.) $\zeta_1(1) = 0.406883388492$, $\zeta_2(1) = 0.091796743420$, $\zeta_3(1) = 3.515225231759$ have been chosen to well-reproduce a Slater function with unit exponent ($\xi = 1$). The primitive Gaussian exponents are thus functions of the Slater exponent and scale according to $\zeta_\gamma(\xi) = \zeta_\gamma(1) \times \xi^2$.

A GME of order $l_{\max}$ contains a total of $(l_{\max} + 1)^2$ functions; all of which share a common Slater exponent ξ and differ only by which (l, μ)-indices are used in the STGO. We refer to a GME by its maximum order, e.g., D refers to a GME of $l_{\max} = 2$. Furthermore, we may use more than one GME on an atom, e.g., 3D, which indicates that there are three GMEs with $l_{\max} = 2$ and each corresponding to one of three Slater exponents. The idea of using more than one GME may initially seem daunting to the reader; however, it has previously been shown[55] that the GME integrals can be computed very efficiently, and the calculation of the Coulomb energy [Eq. (17)] is greatly simplified merely from the fact that an atom will appear as a single point multipole expansion to all nonoverlapping atoms.

D. Computational details

1. Reference models

The application of the theory presented in the preceding sections requires the assessment of some practical questions: How many GMEs are necessary? What maximum angular momentum order do they need to be? What Slater exponents should be used? To answer these questions, we must have a mechanism for judging if an auxiliary basis is "good" or "bad." Our generalization is founded on the principle that an auxiliary basis can reproduce AO products, so we choose to judge the goodness of an auxiliary basis by observing the extent to which the results of a reference model change when $W[\delta\rho, \omega]$ is evaluated with auxiliary functions instead of the AO products. We wish to limit the differences between the models used in our comparisons so that we can make

meaningful attributions of the errors to specific approximations. SCC-DFTB is sufficiently reliant on large empirical corrections that we suspect a successful application of our generalization to it would require even more empiricism or significant changes to those corrections. Therefore, we have chosen to instead use the "VEJ" method introduced in Ref. 10 as our reference model because, not only is it accurate, but the differences between it and standard PBE/6-31G* can be attributed entirely to the Taylor series truncation of the exchange-correlation functional to first order.

The VEJ model is completely described in Ref. 10, however, let us review its functional form. The VEJ model is an all-electron second-order Kohn-Sham potential energy expansion method that evaluates the zeroth and first-order expansion terms without integral approximations, and uses a Coulomb approximation for the second functional derivatives of the Kohn-Sham potential energy. The VEJ model is evaluated using the PBE functional[58] and the AOs and atom reference densities resulting from isolated atom calculations solved with a spherical harmonic 6-31G* basis in the absence of a radial confinement potential. The expression for the VEJ energy is $E_{\mathrm{VEJ}}[\delta\rho,\omega,\mathbf{R}] = E_{\mathrm{TB}}[\delta\rho,\mathbf{R}] + W_{\mathrm{VEJ}}[\delta\rho,\omega]$, where

$$\begin{aligned} E_{\mathrm{TB}}[\delta\rho,\mathbf{R}] = &-\frac{1}{2}\sum_{ij} P_{ij}\int \chi_i(\mathbf{r})\bigtriangledown^2\chi_j(\mathbf{r})d^3r \\ &+ \int \rho_{\mathrm{ref}}(\mathbf{r})\left(v(\mathbf{r}) + \frac{1}{2}\phi_{\mathrm{ref}}(\mathbf{r})\right)d^3r \\ &+ E_{\mathrm{PBE}}[\rho_{\mathrm{ref}}(\mathbf{r}),0] \\ &+ \int \delta\rho(\mathbf{r})\left(v(\mathbf{r}) + \phi_{\mathrm{ref}}(\mathbf{r})\right. \\ &+ \left.\left[\frac{\delta E_{\mathrm{PBE}}[\rho,\omega]}{\delta\rho(\mathbf{r})}\right]_0\right)d^3r, \end{aligned} \tag{34}$$

$v(\mathbf{r}) = -\sum_a Z_a|\mathbf{r}-\mathbf{R}_a|^{-1}$, $\rho_{\mathrm{ref}}(\mathbf{r}) = \sum_a \rho_a(\mathbf{r}-\mathbf{R}_a)$, $\rho_a(\mathbf{r})$ is the atomic density of atom a, $\phi_{\mathrm{ref}}(\mathbf{r}) = \int \rho_{\mathrm{ref}}(\mathbf{r}')|\mathbf{r}-\mathbf{r}'|^{-1}d^3r$, $E_{\mathrm{PBE}}[\rho,\omega]$ is the PBE exchange-correlation functional,[58] and $W_{\mathrm{VEJ}}[\delta\rho,\omega] = J[\delta\rho]$ [Eq. (16)]. When we say that VEJ is the reference model and we make comparison of it to an "auxiliary model," we mean that the auxiliary model is the VEJ model in which $W_{\mathrm{VEJ}}[\delta\rho,\omega]$ is replaced by Eq. (17), i.e., all AO products appearing in the second-order energy are replaced by the auxiliary basis.

The VEJ energy lacks second-order exchange-correlation and is therefore incapable of describing spin-polarization. Our generalization allows for spin-polarized forms of $W(\mathbf{m},\mathbf{s},\mathbf{R})$, and so the reader may prefer that we choose a spin-polarizable reference model. Indeed, we could have chosen to use the "VE" model,[10] which goes one step beyond the VEJ model by including second-order exchange-correlation; however, its evaluation requires more than one- and two-center integrals and thus *completely defeats the purpose of having used the auxiliary basis*. Although a comparison is possible, we want to avoid the appearance of advocating the use of an auxiliary basis with such a Hamiltonian. We limit our examination of second-order exchange-correlation effects for this reason and consider it here only within the confines of a special case. Specifically, we will use the VE model[10] (see below) with auxiliary basis sets to quantify their ability to reproduce the electronegativity and hardness of atoms.

The energy of the VE model is $E_{\mathrm{VE}}[\delta\rho,\omega,\mathbf{R}] = E_{\mathrm{TB}}[\delta\rho,\mathbf{R}] + W_{\mathrm{VE}}[\delta\rho,\omega]$, where

$$\begin{aligned} W_{\mathrm{VE}}[\delta\rho,\omega] = J[\delta\rho] &+ \frac{1}{2}\int \delta\rho(\mathbf{r})^2\left[\frac{\delta^2 E_{\mathrm{SPW92}}[\rho,\omega]}{\delta\rho(\mathbf{r})\delta\rho(\mathbf{r})}\right]_0 d^3r \\ &+ \frac{1}{2}\int \omega(\mathbf{r})^2\left[\frac{\delta^2 E_{\mathrm{SPW92}}[\rho,\omega]}{\delta\omega(\mathbf{r})\delta\omega(\mathbf{r})}\right]_0 d^3r, \end{aligned} \tag{35}$$

and $E_{\mathrm{SPW92}}[\rho,\omega]$ is the SPW92 exchange-correlation functional.[58] When we say that VE is the reference model and we are making a comparison to an "auxiliary model," we mean that the auxiliary model is the VE model in which $W_{\mathrm{VE}}[\delta\rho,\omega]$ is replaced by Eq. (36),

$$\begin{aligned} W_{\mathrm{VE}}(\mathbf{m},\mathbf{s},\mathbf{R}) = &J(\mathbf{m},\mathbf{R}) + \frac{1}{2}\sum_a\sum_b\sum_{k\in a}\sum_{k'\in b} m_k^a m_{k'}^b \\ &\times \int \varphi_k(\mathbf{r}-\mathbf{R}_a)\varphi_{k'}(\mathbf{r}-\mathbf{R}_b) \\ &\times \left[\frac{\delta^2 E_{\mathrm{SPW92}}[\rho,\omega]}{\delta\rho(\mathbf{r})\delta\rho(\mathbf{r})}\right]_0 d^3r \\ &+ \frac{1}{2}\sum_a\sum_b\sum_{k\in a}\sum_{k'\in b} s_k^a s_{k'}^b \\ &\times \int \varphi_k(\mathbf{r}-\mathbf{R}_a)\varphi_{k'}(\mathbf{r}-\mathbf{R}_b) \\ &\times \left[\frac{\delta^2 E_{\mathrm{SPW92}}[\rho,\omega]}{\delta\omega(\mathbf{r})\delta\omega(\mathbf{r})}\right]_0 d^3r. \end{aligned} \tag{36}$$

2. Unoptimized auxiliary basis sets

Before one can optimize the auxiliary Slater exponents, one must first make a decision regarding the number of Slater exponents that are to be be optimized and the maximum order of the GMEs. For this purpose, we examine several auxiliary basis sets in Table I whose exponents *have not* been optimized. The basis sets 1S(M), 1S, 1P, 1D, 1F, and 1G use a single contracted Slater-type GME whose Slater exponent was chosen to reproduce the experimental hardness of the atom, because this is how they are chosen in SCC-DFTB. The mapping coefficients for all auxiliary basis sets in these tables were performed using the procedure described in the previous sections, except for the model using the 1S(M) basis, which instead uses a simple Mulliken partitioning [Eqs. (10) and (11)]. The 6S, 6P, 6D, 6F, and 6G auxiliary basis sets appearing in Table I use six GMEs per atom, and considering that combinations of GMEs can act to form Slater-like representations, each GME is limited to a single, primitive Gaussian instead of being a contracted representation of a Slater function. The primitive Gaussian exponents of the 6S-6G basis *have not* been optimized. Instead, every atom has the exact same set of six Gaussian exponents: 10, 5, 2.5, 1, 0.4, and 0.1 a.u..

TABLE I. Fixed-geometry response property mean unsigned errors. The average reference dipole and quadrupole moment vector norms are 0.453 and 1.758 a.u., respectively, the average integral of the response density magnitude is 1.077 a.u, and the mean unsigned reference W and E_{resp} values are 31.332 and 115.840 mE_h, respectively. The column "N" displays the number of molecules included in the statistics. A value of N less than 52 indicates that some molecules do not SCF converge.

Model	N	$\lvert\Delta\mathbf{q}^{(1)}\rvert$	$\lvert\Delta\mathbf{q}^{(2)}\rvert$	$\lvert\Delta\rho_{\text{VEJ}}\rvert$	$\lvert\Delta W\rvert$	$\lvert\Delta E_{\text{resp}}\rvert$
1S(M)	52	0.215	1.230	1.021	25.872	42.077
1S	51	0.301	1.485	1.024	27.683	45.153
1P	49	0.110	1.217	1.038	14.566	20.942
1D	47	0.103	0.372	0.937	16.434	18.511
1F	47	0.108	0.347	0.859	16.626	18.777
1G	46	0.105	0.339	0.865	16.791	19.120
6S	33	0.211	1.359	0.949	10.419	12.931
6P	49	0.043	1.080	0.712	5.804	6.772
6D	52	0.006	0.037	0.238	1.113	1.703
6F	52	0.003	0.030	0.138	0.142	0.207
6G	52	0.003	0.030	0.121	0.122	0.193
2P,3D,4F	52	0.012	0.072	0.551	0.662	1.105

3. Optimized auxiliary basis sets

Based on the 1S-1G and 6S-6G results shown in Table I, we have chosen several auxiliary basis sets whose Slater exponents were optimized in a nonlinear fitting procedure described below. We defer most of our discussion to Sec. III, but to understand our notation, let us briefly summarize some of our arguments and observations. As one traverses down the rows of the periodic table, the number of AOs increases, their radial behavior becomes more complicated, and the oscillatory nature of the AO products are further compounded. From this argument and from our experience, this requires a corresponding increase in the number of GMEs necessary to describe the AO products for heavier elements. To denote this, let the GMEs for period 1, 2, and 3 elements be separated by commas, e.g., "2P,3D,4F" indicates that period 1 elements (H-He) use a 2P GME basis, period 2 elements (Li-Ne) use a 3D GME basis, and period 3 elements (Na-Ar) use a 4F GME basis. The 2P,3D,4F auxiliary basis appearing in the tables and figures of this manuscript are what we consider to be the final outcome of our parametrization.

Following Ref. 10, we examine the errors of several properties (Tables I–II) using the statistics gathered from 52 molecules[59] taken from the G2/97 neutral small molecule test set.[60] The parametrization began by first fitting the Slater exponents of H, C, N, and O to a subset of these molecules, and then optimizing the exponents of the other atoms while fixing the values of H, C, N, and O. The parametrization consists of (1) choosing a trial set of Slater exponents, (2) using those exponents to perform SCF calculations on a pre-defined set of molecules, whose coordinates are fixed to the standard PBE/6-31G* optimized geometries, and then (3) computing a set of quantities derivable from the response density and comparing those to the corresponding VEJ-computed values. The process is repeated until no better fit is found, and the merit function that we have used to evaluate the fit is

$$\chi^2 = \sum_{i=1}^{N_{\text{mol}}} 20|\Delta\mathbf{q}^{(1)}|_i + 3|\Delta\mathbf{q}^{(2)}|_i + 500|\Delta W|_i + 500|\Delta E_{\text{resp}}|_i + |\Delta\rho_{\text{VEJ}}|_i + \frac{1}{2}|\Delta\rho_{\text{Model}}|_i, \tag{37}$$

where $|\Delta\mathbf{q}^{(1)}|$ is the vector-norm of the difference between the model and VEJ-computed dipole moments, i.e., the dipole moment magnitude of the model and VEJ-computed difference density, $|\Delta\mathbf{q}^{(2)}|$ is the vector-norm of the quadrupole moment difference,

$$E_{\text{resp}} = E_{\text{scf}} - V^{(0)}(\mathbf{R}) - \sum_{ij} P_{ij}^{(0)} T_{ij} \tag{38}$$

is a "response energy" and $|\Delta E_{\text{resp}}|_i$ is the absolute difference between the model and VEJ response energies of molecule i.

$$|\Delta W|_i = |J(\mathbf{m}_{\text{Model},i}, \mathbf{R}) - J[\delta\rho_{\text{VEJ},i}]| \tag{39}$$

is the difference between the auxiliary model and VEJ response density Coulomb self-energies of molecule i.

The final quantities to be explained in Eq. (37),

$$|\Delta\rho_{\text{VEJ}}| = \int |\Delta\rho_{\text{VEJ}}(\mathbf{r})| d^3r \tag{40}$$

and

$$|\Delta\rho_{\text{Model}}| = \int |\Delta\rho_{\text{Model}}(\mathbf{r})| d^3r, \tag{41}$$

TABLE II. Bond, angle, and dipole moment errors for the full set of 52 molecules upon geometry optimization. The statistics under the heading ΔE_{rxn} are adiabatic SCF energy differences corresponding to the homolytic bond dissociation reactions: $C_2H_6 \rightarrow 2CH_3$, $C_2H_4 \rightarrow 2CH_2$, $C_2H_2 \rightarrow 2CH$, $N_2H_4 \rightarrow 2NH_2$, $Si_2H_6 \rightarrow 2SiH_3$, and $H_2O_2 \rightarrow 2OH$. μ_{SE} and μ_{UE} are the signed and unsigned errors of the property, respectively, and whose units are shown in the row "Avg.," which displays the average reference value. "N" is the amount of data included in the statistics.

	Bond		Angle		Dipole		ΔE_{rxn}	
N	114		98		52		6	
Avg.	1.334 Å		112.348°		0.451 a.u.		158.637 kcal/mol	
	μ_{SE}	μ_{UE}	μ_{SE}	μ_{UE}	μ_{SE}	μ_{UE}	μ_{SE}	μ_{UE}
1S(M)	−0.057	0.058	0.582	1.307	−0.162	0.213	21.577	21.577
2P,3D,4F	0.001	0.002	−0.060	0.236	0.005	0.013	−0.015	1.452

quantify the absolute difference in response densities, i.e.,

$$\Delta\rho_{\mathrm{X}}(\mathbf{r}) = -\sum_{a}\sum_{k} m_k^{a,\mathrm{Model}}\varphi_k(\mathbf{r}-\mathbf{R}_a) - \sum_{ij}\left(P_{ij}^{\mathrm{X}} - P_{ij}^{(0)}\right)\chi_i(\mathbf{r})\chi_j(\mathbf{r}), \quad (42)$$

where the subscript "X" in $\Delta\rho_{\mathrm{X}}(\mathbf{r})$ is either "VEJ" or "Model," which indicates whether the difference density is respect to the auxiliary model-computed density matrix $\mathbf{P}^{\mathrm{Model}}$ or the VEJ-computed density matrix $\mathbf{P}^{\mathrm{VEJ}}$.

4. Nonbonded interactions: The water dimer

Figure 2 displays the standard PBE/6-31G* [2(a)] and VEJ [2(d)] water dimer interaction energy, i.e., $\Delta E = E(2\mathrm{H_2O}) - 2E(\mathrm{H_2O})$, as a two-dimensional function of oxygen position relative to a stationary water. Figures 2(b) and 2(c) are the difference in interaction energies, i.e., $\Delta\Delta E = \Delta E_{\mathrm{model}} - \Delta E_{\mathrm{ref}}$, for 1S(M) and 2P,3D,4F, respectively, relative to standard PBE/6-31G*. Figures 2(e) and 2(f) are analogous differences with respect to VEJ. Each colored square in Fig. 2 represents a calculation in which the three atoms of a stationary water are fixed in space (shown explicitly) and the oxygen of a second water molecule is placed in the plane formed by the three atoms of the first. The position (Å) of the oxygen atom is represented by the x- and y-axis in Fig. 2. The position of the hydrogens in the second water are allowed to geometry optimize under the constraint that the internal geometry of the water preserves the PBE/6-31G* isolated water structure. Thus, each calculation involves a geometry optimization of a water dimer system having only three degrees of freedom: the orientation and "twist" of the C_2 axis of the second water.

5. Second-order exchange-correlation effects

Table III examines the effect of including second-order exchange-correlation on the Mulliken electronegativity[61] χ_{M} and Pearson hardness[62] η_{P} of atoms, and of the ability of the 1S(M) and 2P,3D,4F basis sets to reproduce those effects when the second-order energy is replaced with expressions involving the auxiliary basis functions. The Mulliken electronegativity of an atom is $\chi_{\mathrm{M}} = (\mathrm{IP} + \mathrm{EA})/2$, where IP and EA are the ionization potential and electron affinity of the atom, which are trivially related to the energy of the atom and its ions. The Pearson hardness of an atom is $\eta_{\mathrm{P}} = (\mathrm{IP} - \mathrm{EA})/2$. To determine the effect of second-order exchange-correlation on these quantities, we compute $\Delta\chi_{\mathrm{M}} = \chi_{\mathrm{M}}^{\mathrm{VE}} - \chi_{\mathrm{M}}^{\mathrm{VEJ}}$ and $\Delta\eta_{\mathrm{P}} = \eta_{\mathrm{P}}^{\mathrm{VE}} - \eta_{\mathrm{P}}^{\mathrm{VEJ}}$, which are simply the differences in these quantities when we turn on (VE) and turn off (VEJ) second-order exchange-correlation contributions to the energy. These shifts can be computed from models that evaluate the second-order terms using the AO products, which we consider to be the "target" values. Similarly, the shifts can be evaluated using models that evaluate the second-order terms with an auxiliary basis, and the statistics in this table compare these shifts to the target values.

TABLE III. The effect of second-order exchange-correlation on the Mulliken electronegativity and Pearson hardness of the atoms, and the ability of the 1S(M) and 2S,3P,4D auxiliary basis sets to reproduce these effects. The statistics reflect the properties of H, Be, C, N, O, F, Si, P, S, and Cl.

Avg.	$\Delta\chi_{\mathrm{M}}$ -13.262 mE$_h$		$\Delta\eta_{\mathrm{P}}$ -9.156 mE$_h$	
	μ_{SE}	μ_{UE}	μ_{SE}	μ_{UE}
1S(M)	−12.353	13.170	4.076	7.123
2P,3D,4F	−0.810	0.968	0.131	1.167

TABLE IV. Timings (microseconds) of the pre-SCF calculation of $\mathbf{M}^a$ and $\mathbf{M}^b$ from spline evaluation and subsequent rotation using Eq. (25). These timings include the evaluation of the Wigner-D matrices. The mapping coefficient matrices have dimensions $N_{\mathrm{AO}}^2 N_{\mathrm{aux}}$ and thus their timing depends on the chosen combination of AO and auxiliary basis sets.

	Auxiliary basis					
AO	1S	1P	1D	2P	2D	3D
1s1p	0.7	2.7	7.6	5.7	11.8	18.5
2s1p	0.8	3.4	8.0	6.4	13.7	20.5
2s2p	1.1	5.5	14.0	11.2	27.0	41.5
1s1p1d	3.2	12.2	28.0	23.8	56.5	85.3
3s2p1d	4.8	16.8	41.1	33.4	83.5	124.4

6. Computational effort

Tables IV–V report wall clock times required to compute the mapping coefficients [Eq. (25)] and Coulomb energy and potential [Eqs. (17) and (21)], respectively, for a pair of atoms. These timings were performed on a single Intel Xeon E5520 2.26GHz processing core. The computer code was written in Fortran 90 and compiled with the Intel Fortran Compiler Version 11.1 with the compilation flags "-xHost -O3." Table IV reports the times as a function of both AO and auxiliary basis, and much of our discussion will focus on the 1s1p minimal valence timings, as opposed to the 6-31G* timings, since we suspect that most readers will be interested in AO basis sets similar to what SCC-DFTB currently uses.

III. RESULTS AND DISCUSSION

A. Unoptimized auxiliary basis sets

As explained in Ref. 10, there are a number of differences between the VEJ model and SCC-DFTB; however, the 1S(M)

TABLE V. Timings (microseconds) of GME Coulomb auxiliary potential and energy evaluation [Eqs. (17) and (21)] for primitive Gaussians (K=1) and contracted Slater-like functions (K=3).

	Auxiliary basis					
K	1S	1P	1D	2P	2D	3D
1	0.1	0.2	0.5	0.7	1.8	3.9
3	0.7	1.0	1.3	3.6	5.2	11.5

auxiliary basis and its usage of Mulliken charge mapping is consistent with SCC-DFTB's treatment of electrostatics. Extending the Slater-monopole representation of the response density to include higher-order multipoles is, perhaps, what one might first try as being the simplest possible improvement, and it is for this reason that we include the 1S-1G results in Table I. We observe SCF convergence difficulties in the 1S-1G series as the angular momentum order is increased. Alternatively, the 6S-6D series shows SCF convergence difficulties only with low angular momentum orders. These observations result from two underlying issues: (1) When there is too little radial completeness, the multipole moment constraints can cause erroneous behavior near the nuclei (e.g., having the wrong "sign") because the constraints enforce the long-range decay behavior of the AO-products with a weight of r^l, which renders the short-range behavior insignificant with increasing l. (2) When there is a large degree of radial completeness, but too little angular completeness, some AO products are well represented by the auxiliary basis, whereas others are not. We have come to conclude that achieving a uniform balance of electron repulsions is more important than making incremental improvements that can upset the balance of competing repulsive electronic forces. Furthermore, we have come to believe that the success of 1S(M) in SCC-DFTB is likely due to the fact that it so poorly represents all AO products that it avoids encountering the instabilities arising from the strong repulsions between a large number of different AO products.

B. Optimized auxiliary basis sets

We chose the 2P,3D,4F basis by partitioning the molecules into two subsets: molecules containing period 2 elements and molecules containing period 3 elements, and we then examined the the 6S-6G series of errors for each subset. The "period 2"-subset produced acceptably small E_{resp} errors (1 mE_h) for D-type and higher GMEs, whereas period 3 elements required F-type GMEs to achieve that accuracy. Furthermore, we encountered SCF convergence difficulties when we used fewer than three D-type GMEs on period 2 elements and four F-type GMEs on period 3 elements. To further justify our use of the 2P,3D,4F basis, we parametrized other auxiliary basis sets that increment and decrement some of the GME orders, and we have also tried including an extra P-type GME on period 2 elements, but these methods did not offer significant improvement.

Table I compares the statistics between 1S(M) and 2P,3D,4F for the full set of 52 molecules that we've considered. The 2P,3D,4F basis reduces the multipole moment errors relative to 1S(M) by more than a factor of ten, and yields E_{resp} errors of approximately 1 mE_h when compared to VEJ.

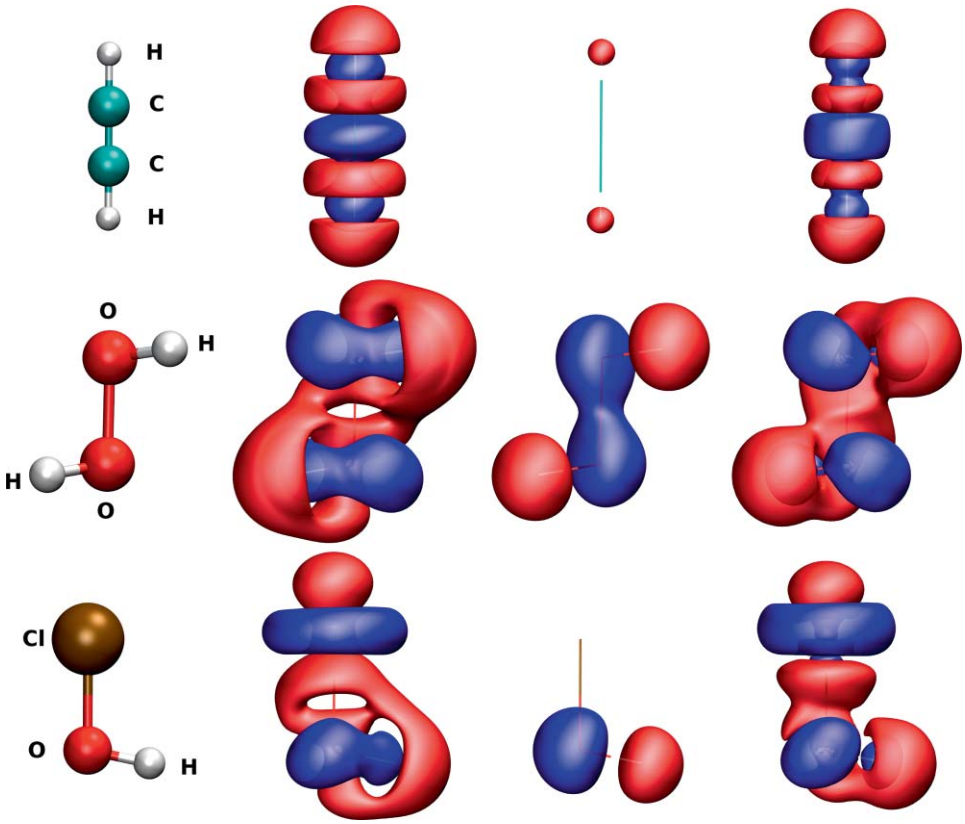

FIG. 1. Three-dimensional density response isocontour surfaces of the molecules shown in the left column using VEJ (second column), 1S(M) (third column), and 2P,3D,4F (fourth column). The contour levels are ±0.004 (C_2H_2), ±0.007 (H_2O_2), and ±0.007 (HOCl) atomic units. Positive contours are blue and indicate an increase in electron density upon SCF convergence relative to the sum of isolated atom densities. The isocontours have a slight transparency that allow for a better view of the interior behavior. The magnitude of the 1S(M) response is so much smaller than that of VEJ and 2P,3D,4F that the 1S(M) figures artificially appear as though their response was not charge balanced. Reducing the isocontour values further, to better illustrate the 1S(M) response, would render the VEJ and 2P,3D,4F figures completely illegible.

We find these results encouraging, and suspect that the errors could be reduced further had we allowed the GME primitive exponents and contraction coefficients to optimize freely, as opposed to being restricted to a Slater-like representation. This would allow for the possibility of including oscillatory behavior directly in the auxiliary basis instead of solely relying on linear combinations of GMEs to create the effect.

The differences between the 1S(M) and 2P,3D,4F basis sets may be better appreciated through the qualitative comparison shown in Fig. 1. In this figure, one can see that the 2P,3D,4F basis reproduces the complicated nodal structure of the response density in ethyne, the lone-pair lobe of sp^3-hybridized oxygen, and the D-response on chlorine. The 1S(M) isocontour surfaces lack all of the above listed characteristics.

To more fully compare the 1S(M) and 2P,3D,4F auxiliary basis models to VEJ, we display some geometric and energetic statistics produced upon geometry optimization in Table II. The 2P,3D,4F bond length errors are trivially small, the angle errors are a factor of six smaller than 1S(M), and the dipole moment errors are reduced by a factor of sixteen. 2P,3D,4F accurately reproduces the VEJ adiabatic bond energies to within 1% of the average reference value, and is 20 kcal/mol better than 1S(M).

C. Nonbonded interactions: The water dimer

The above comparisons were limited to isolated molecule properties, so to examine the extent to which the auxiliary basis affects nonbonded interactions, Fig. 2 compares the 1S(M), 2P,3D,4F, and VEJ interaction energy surfaces of a water dimer. The 2P,3D,4F basis reproduces the VEJ interaction surface very well, whereas the 1S(M) basis yields errors of approximately 4 mE_h in the region near the minimum energy configuration of the dimer. Our only purpose for displaying the PBE/6-31G* interaction energy is to show the reader how well VEJ reproduces it, for if VEJ had carried the expansion of the exchange-correlation functional to infinite order, we would expect it to exactly reproduce PBE/6-31G*. The errors of 1S(M) persist in both comparisons, therefore the auxiliary basis and Taylor series truncation do not offset in a "happy-cancellation" of errors.

D. Second-order exchange-correlation effects

Table III examines how the electronegativity and hardness of atoms are changed when the second-order exchange-correlation (including spin-polarization) is included in the model. The 1S(M) auxiliary basis poorly reproduces the shifts

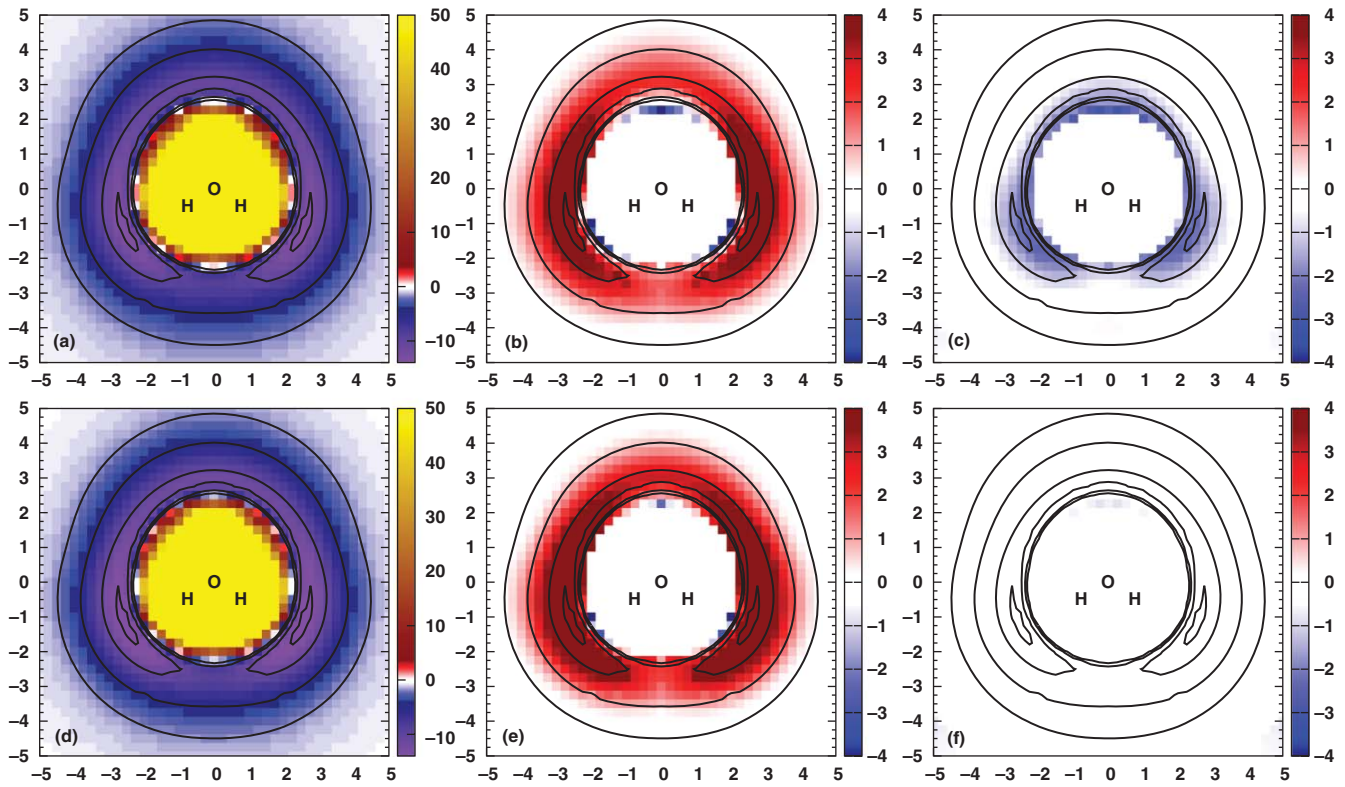

FIG. 2. Water dimer interaction energies. The letters "O" and "H" are the position of the first water's atoms, and the x- and y-axis (Å) indicate the position of the second water's oxygen atom. The numerical values of the color scale represent either an interaction energy or an interaction energy difference in units of mE_h. The standard PBE [(a)] and VEJ [(d)] interaction energies are differences in their total energies minus the sum of the monomer energies. The 1S(M) [(b)] and 2P,3D,4F [(c)] plots are the difference between their interaction energies and the standard PBE interaction energies, i.e., these are $\Delta\Delta E$'s. Parts (e) and (f) are analogous to (b) and (c), respectively: they are differences with respect to the VEJ interaction energies. All parts use the *same* water dimer geometries; the geometry optimizations were performed once with standard PBE/6-31G* and the energy of all models were evaluated at those geometries. The absolute scale in parts (a) and (d) differ from the other parts, but the scales used in all parts are color-consistent. The solid lines appearing in all parts of the figure are contour lines taken from the PBE/6-31G* interaction energy plot, and serve no purpose other than to aid the reader's eye when comparing the location of colors between the plots.

in these quantities, whereas the 2P,3D,4F basis matches the AO product-computed shifts with an accuracy of 1 mE_h.

E. Computational effort

Our generalization formally scales quadratically with respect to system size and scales linearly for large systems when cutoffs and fast multipole methods become accurate and economical; however, it is of interest to gain a better perspective of the computational cost for small systems. There are two aspects here that would contribute significantly to the execution speed of an SCC-DFTB-like computer program: (1) the calculation of $\mathbf{M}^a$ and $\mathbf{M}^b$, and (2) the calculation of Eqs. (17) and (21) with a GME basis. The wall clock time required to compute these quantities for a pair of atoms is shown in Tables IV–V, respectively. By reporting the times for a pair of atoms, one can approximate the cost of computing $\mathbf{M}^a$ and $\mathbf{M}^b$ for an N-atom system by multiplying the times listed in the table by $N(N-1)/2$. The times in Table V depend on the number of SCF iterations required to reach convergence, so the contribution of these times to the total execution time of the program would be approximately $N_{\text{iter}}N(N-1)/2$.

$\mathbf{M}^a$ and $\mathbf{M}^b$ only need to be computed once before the SCF procedure begins, but it is obviously not the only thing that would be pre-computed in a typical SCF program, and so a doubling of times in Table IV does not indicate that the computer program would halve its net speed. Before the SCF begins, a typical program would also pre-compute the symmetric orthogonalization matrix $\mathbf{S}^{-1/2}$ from the overlap matrix, as this would be needed to transform the generalized eigenvalue problem [Eq. (6)] into a standard eigenvalue problem within every SCF cycle. This operation scales cubically with respect to the number of AOs; however, for a system of 5–15 heavy atoms with a 1s1p AO basis, its calculation requires approximately the same wall clock time as it does to compute *all* of the mapping coefficients with a 1D auxiliary basis (not just those for a pair of atoms). Therefore, although the 1s1p row in Table IV shows that it is 10 times more expensive to compute the 1D mapping coefficients than the 1S mapping coefficients, this would slow the pre-SCF part of the calculation by only a factor of two.

The timings in Table V are similar to those shown in Ref. 55; the algorithm used here is a direct implementation of what has previously been described. We note that the 1D Slater-like functions are twice as slow as the 1S timings; however, the Fock matrix must be diagaonlized at every iteration as well, and so a doubling of times in Table V does not mean that the SCF cycles will halve their net speed. This, along with our discussion of Table IV, suggests to us that extending SCC-DFTB to quadrupoles would slow it down by no more than one-half. We emphasize that we are trying to be conservative with our estimate, and we would not be surprised if it performed even better.

IV. CONCLUSION

We have generalized the formulation of Kohn-Sham potential energy expansion methods to include arbitrary single-center auxiliary basis sets whose mapping coefficients can be pretabulated and splined as a function of dimer separation and rotated into the molecular orientation. A procedure for determining the mapping coefficients from a multipole moment constrained electrostatic fitting procedure has been described. We have used the above methods with GMEs to realize the computational advantages of the recently developed integral method in Ref. 55, and we explored the effect of GME angular momentum and radial completeness on its ability to reproduce AO-computed response properties. Furthermore, we parametrized the Slater exponents of an auxiliary basis, and it was shown to produce quantitatively correct density responses, and it reduced the errors of bond lengths, angles, and covalent bond strengths. The parametrized basis and a SCC-DFTB-like monopolar auxiliary basis were used to compute the potential energy surface of a water dimer, and it was shown that the hydrogen bond strength of the water dimer was underestimated when the density response was treated with monopolar functions, and this underestimation was corrected when multipolar auxiliary functions were used.

The present work is a significant advance in Kohn-Sham expansion methods and promises a route toward improved intra- and intermolecular interactions; however, this is not the proverbial end of the road. At its current stage, the VEJ method with an auxiliary basis is more akin to an *ab initio* method than a semiempirical method because it lacks a computationally efficient approximation for the first-order matrix elements. Granted, the first-order matrix elements need only be computed *once* before the SCF procedure begins; however, a truly efficient semiempirical method should overcome the use of quadrature altogether,[63] but this is a subject we must defer to future work.

Another possible direction for future work would be to directly apply the auxiliary basis generalization presented here to SCC-DFTB. We suspect that fewer auxiliary functions would be necessary in SCC-DFTB since it uses a minimal valence basis. Thus there should be less need to incorporate the radial completeness that would otherwise be necessary to distinguish between products of similar AOs, e.g., 1s, 2s, 3s, etc., as is the case with an all-electron 6-31G* basis. Improving the AO product density electron repulsions would only address one of the three major approximations listed in the introduction, and so a simple implementation of this generalization may not yield an overall improved SCC-DFTB model without additional empiricism. Note that our previous work[10] suggested that, if the first-order matrix elements are computed using a two-body approximation, a complete auxiliary basis would yield molecular dipole moment errors of approximately the same magnitude as a Slater monopole basis when evaluated at standard DFT geometries.

ACKNOWLEDGMENTS

The authors are grateful for financial support provided by the National Institutes of Health (GM084149). Computational resources from the Minnesota Supercomputing Institute for Advanced Computational Research (MSI) were utilized in this work. This research was supported in part by the National Science Foundation through TeraGrid resources

provided by the National Center for Supercomputing Applications and the Texas Advanced Computing Center under Grant TG-CHE100072.

[1]M. Elstner, T. Frauenheim, E. Kaxiras, G. Seifert, and S. Suhai, Phys. Status Solidi. B **217**, 357 (2000).
[2]Q. Cui, M. Elstner, E. Kaxiras, T. Frauenheim, and M. Karplus, J. Phys. Chem. B **105**, 569 (2001).
[3]M. Elstner, Theor. Chem. Acc. **116**, 316 (2006).
[4]Y. Yang, H. Yu, D. M. York, Q. Cui, and M. Elstner, J. Phys. Chem. A **111**, 10861 (2007).
[5]N. Otte, M. Scholten, and W. Thiel, J. Phys. Chem. A **111**, 5751 (2007).
[6]K. W. Sattelmeyer, J. Tirado-Rives, and W. L. Jorgensen, J. Phys. Chem. A **110**, 13551 (2006).
[7]O. V. Shishkin, L. Gorb, A. V. Luzanov, M. Elstner, S. Suhai, and J. Leszczynski, J. Mol. Struct.: THEOCHEM **625**, 295 (2003).
[8]H. Zhou, E. Tajkhorshid, T. Frauenheim, S. Suhai, and M. Elstner, Chem. Phys. **277**, 91 (2002).
[9]Y. Yang, H. Yu, D. York, M. Elstner, and Q. Cui, J. Chem. Theory Comput. **4**, 2067 (2008).
[10]T. J. Giese and D. M. York, J. Chem. Phys. **133**, 244107 (2010).
[11]M. Gaus, Q. Cui, and M. Elstner, J. Chem. Theory Comput. **7**, 931 (2011).
[12]S. Kaminski, M. Gaus, P. Phatak, D. von Stetten, M. Elstner, and M. A. Mroginski, J. Chem. Theory Comput. **6**, 1240 (2010).
[13]D. Riccardi, G. Li, and Q. Cui, J. Phys. Chem. B **108**, 6467 (2004).
[14]A. Kumar, M. Elstner, and S. Suhai, Int. J. Quantum Chem. **95**, 44 (2003).
[15]Z.-L. Cai, P. Lopez, J. R. Reimers, Q. Cui, and M. Elstner, J. Phys. Chem. A **111**, 5743 (2007).
[16]M. Elstner, Q. Cui, P. Munih, E. Kaxiras, T. Frauenheim, and M. Karplus, J. Comput. Chem. **24**, 565 (2003).
[17]G. Dolgonos, B. Aradi, N. H. Moreira, and T. Frauenheim, J. Chem. Theory Comput. **6**, 266 (2010).
[18]G. Zheng, H. A. Witek, P. Bobadova-Parvanova, S. Irle, D. G. Musaev, R. Prabhakar, and K. Morokuma, J. Chem. Theory Comput. **3**, 1349 (2007).
[19]R. C. Walker, M. F. Crowley, and D. A. Case, J. Comput. Chem. **29**, 1019 (2008).
[20]G. Seabra, R. C. Walker, M. Elstner, D. A. Case, and A. E. Roitberg, J. Phys. Chem. A **111**, 5655 (2007).
[21]A. T. Paxton and J. J. Kohanoff, J. Chem. Phys. **134**, 044130 (2011).
[22]J.-P. Piquemal, N. Gresh, and C. Giessner-Prettre, J. Phys. Chem. A **107**, 10353 (2003).
[23]J. Piquemal, H. Chevreau, and N. Gresh, J. Chem. Theory Comput. **3**, 824 (2007).
[24]H. Hu, Z. Lu, M. Elstner, J. Hermans, and W. Yang, J. Phys. Chem. A **111**, 5685 (2007).
[25]B. I. Dunlap, N. Rösch, and S. B. Trickey, Mol. Phys. **108**, 3167 (2010).
[26]B. I. Dunlap, J. Mol. Struct.: THEOCHEM, **529**, 37 (2000).
[27]F. Weigand, M. Kattannek, and R. Ahlrichs, J. Chem. Phys. **130**, 164106 (2009).
[28]F. Aquilante, L. Gagliardi, T. B. Pedersen, and R. Lindh, J. Chem. Phys. **130**, 154107 (2009).
[29]Y. Jung, A. Sodt, P. W. Gill, and M. Head-Gordon, Proc. Natl. Acad. Sci. U.S.A. **102**, 6692 (2005).
[30]G. R. Ahmadi and J. Almlöf, Chem. Phys. Lett. **246**, 364 (1995).
[31]G. A. Cisneros, J. Piquemal, and T. A. Darden, J. Chem. Phys. **125**, 184101 (2006).
[32]D. M. Elking, G. A. Cisneros, J. Piquemal, T. A. Darden, and L. G. Pedersen, J. Chem. Theory Comput. **6**, 190 (2010).
[33]J. Piquemal, G. Cisneros, P. Reinhardt, N. Gresh, and T. A. Darden, J. Chem. Phys. **124**, 104101 (2006).
[34]N. Gresh, G. A. Cisneros, T. A. Darden, and J.-P. Piquemal, J. Chem. Theory Comput. **3**, 1960 (2007).
[35]A. Sodt, J. E. Subotnik, and M. Head-Gordon, J. Chem. Phys. **125**, 194109 (2006).
[36]R. T. Gallant and A. St-Amant, Chem. Phys. Lett. **256**, 569 (1996).
[37]F. Aquilante, R. Lindh, and T. B. Pedersen, J. Chem. Phys. **127**, 114107 (2007).
[38]A. M. Burow, M. Sierka, and F. Mohamed, J. Chem. Phys. **131**, 214101 (2009).
[39]M. A. Watson, P. Sałek, P. Macak, and T. Helgaker, J. Chem. Phys. **121**, 2915 (2004).
[40]T. J. Giese and D. M. York, J. Comput. Chem. **29**, 1895 (2008).
[41]C. A. White, B. G. Johnson, P. M.W. Gill, and M. Head-Gordon, Chem. Phys. Lett. **230**, 8 (1994).
[42]W. M.C. Foulkes and R. Haydock, Phys. Rev. B **39**, 12520 (1989).
[43]D. Porezag, G. Jungnickel, J. Elsner, M. Haugk, T. Frauenheim, S. Suhai, and G. Seifert, Phys. Rev. B **58**, 7260 (1998).
[44]G. Seifert, J. Phys. Chem. A **111**, 5609 (2007).
[45]W. Kohn and L. Sham, Phys. Rev. A **140**, A1133 (1965).
[46]C.C. J. Roothaan, Rev. Mod. Phys. **23**, 69 (1951).
[47]S. F. Boys, Proc. R. Soc. London A Mat. **200**, 542 (1950)
[48]C. A. White and M. Head-Gordon, J. Chem. Phys. **104**, 2620 (1996).
[49]Y. Shao, C. A. White, and M. Head-Gordon, J. Chem. Phys. **114**, 6572 (2001).
[50]R. Ahlrichs, Phys. Chem. Chem. Phys. **6**, 5119 (2004).
[51]R. S. Mulliken, J. Am. Chem. Soc. **72**, 4493 (1950).
[52]J. A. Kalinowski, B. Lesyng, J. D. Thompson, C. J. Cramer, and D. G. Truhlar, J. Phys. Chem. A **108**, 2545 (2004).
[53]C. H. Choi, J. Ivanic, M. S. Gordon, and K. Ruedenberg, J. Chem. Phys. **111**, 8825 (1999).
[54]B. I. Dunlap, J. Chem. Phys. **78**, 3140 (1983).
[55]T. J. Giese and D. M. York, J. Chem. Phys. **128**, 064104 (2008).
[56]E. W. Hobson, Proc. London Math. Soc. **24**, 55 (1892).
[57]A. W. Niukkanen, J. Math. Phys. **24**, 1989 (1983).
[58]J. P. Perdew and Y. Wang, Phys. Rev. B **45**, 13244 (1992).
[59]The molecules in the test set are: BeH, C_2H_2, C_2H_4, C_2H_6, CH_2, CH_3, CH_4, CH_4O, CH_4S, CH_3Cl, CN, CS, HC, HCN, HCO, HF, HCl, LiH, NH, HO, H_2O, H_2O_2, OCl, NO, OS, O_2, CO, SiO, CO_2, SO_2, F_2, Cl_2, FCl, Li_2, LiF, Na_2, NaCl, N_2, NH_2, NH_3, N_2H_4, HOCl, H_2CO, P_2, PH_2, PH_3, S_2, H_2S, SiH_2, SiH_3, SiH_4, and Si_2H_6.
[60]L. A. Curtiss, K. Raghavachari, P. C. Redfern, and J. A. Pople, J. Chem. Phys. **106**, 1063 (1997).
[61]R. S. Mulliken, J. Chem. Phys. **2**, 782 (1934).
[62]R. G. Parr and R. G. Pearson, J. Am. Chem. Soc. **105**, 7512 (1983).
[63]Y. Tu, S. P. Jacobsson, and A. Laaksonen, Phys. Rev. B **74**, 205104 (2006).